LABORATORY OF BIOMEDICAL AND ENVIRONMENTAL SCIENCES
900 VETERAN AVENUE
UNIVERSITY OF CALIFORNIA, LOS ANGELES, CALIFORNIA 90024
AND DEPARTMENT OF RADIOLOGICAL SCIENCES
UCLA SCHOOL OF MEDICINE, LOS ANGELES, CALIFORNIA 90024

These studies were supported by Contract #DE-AM03-76-SF00012 between the U.S. Department of Energy and the University of California

Prepared for the U.S. Department of Energy
under Contract #DE-AM03-76-SF00012

The Deoxyglucose Method for the Estimation of Local Myocardial Glucose Metabolism with Positron Computed Tomography

Osman Ratib, M.D., Michael E. Phelps, Ph.D., Sung-Cheng Huang, D.Sc., Eberhard Henze, M.D., Carl E. Selin, M.S. and Heinrich R. Schelbert, M.D.

THE DEOXYGLUCOSE METHOD FOR THE ESTIMATION OF LOCAL MYOCARDIAL GLUCOSE METABOLISM WITH POSITRON COMPUTED TOMOGRAPHY

Osman Ratib, M.D., Michael E. Phelps, Ph.D., Sung-Cheng Huang, D.Sc., Eberhard Henze, M.D., Carl E. Selin, M.S. Heinrich R. Schelbert, M.D.

Divisions of Biophysics and Nuclear Medicine
Department of Radiological Sciences
UCLA School of Medicine
and the
Laboratory of Biomedical and Environmental Sciences
University of California at Los Angeles
Los Angeles, California

Supported in part by Department of Energy contract DE-AM06-76-SF000012, and the Swiss National Foundation of Research (Dr. Ratib)

Direct correspondence to:
Michael E. Phelps, Ph.D.
Division of Biophysics
Department of Radiological Sciences
UCLA School of Medicine
Los Angeles, CA 90024

ABSTRACT

The deoxyglucose method originally developed for measurements of the local cerebral metabolic rate for glucose has been investigated in terms of its application to studies of the heart with positron computed tomography (PCT) and FDG. Studies were performed in dogs to measure the tissue kinetics of FDG with PCT and by direct arterial-venous sampling. The operational equation developed in our laboratory as an extension of the Sokoloff model was used to analyze the data. Error propagation, primarily from corrections applied to remove spillover of activity from the myocardial blood pool to tissue and from partial volume effects in the PCT images, limited the accuracy of estimating the individual rate constant for transport, phosphorylation and dephosphorylation. However, a constant representing the combination of transport and phosphorylation was accurately determined and yielded measured values of the myocardial metabolic rate for glucose (MMRGlc) that were in good agreement with direct determinations using the Fick method over a wide range of glucose metabolic rates (from 1.7 to 21.1 mg/min/100gm). An accurate and stable value of the lumped constant (0.67 ± 0.10) was also found over this range of metabolism. The FDG method accurately predicted the true MMRGlc even when the glucose metabolic rate was normal but myocardial blood flow (MBF) was elevated 5 times the control value or when metabolism was reduced to 10% of normal and MBF increased 5 times normal. Improvements in PCT resolution are required to improve the accuracy of the estimates of the rate constants and the MMRGlc.

With the recent development of positron computed tomography (PCT), cross-sectional imaging of the heart has become possible (1,2). These cross-sectional images reflect quantitatively the distribution of radioactive tracer concentrations in myocardium and thus resemble in vivo autoradiographs. This new imaging approach provides a potential nontraumatic means of quantitating regional myocardial metabolism using tracer kinetic models.

Sokoloff et al (3) recently developed an autoradiographic method and tracer kinetic model for the measurement of the local cerebral metabolic rate for glucose using the C-14 labeled glucose analog, 2-deoxyglucose. The 2-deoxyglucose has been labeled with fluorine-18 by Ido et al (4) to form 2-fluoro-2-deoxy-D-glucose (FDG). FDG has been shown by Bessell et al (5), Gallagher et al (6), Reivich et al (7) and Machado DeDomenech and Sols (8) to be a substrate for hexokinase with the end product being FDG-6-PO_4. Phelps et al (9) and Huang et al (10) have shown that the transport and phosphorylation constants for FDG in the brain of man are similar to those for DG in the monkey (11) and somewhat lower than values in the rat (3) because of the higher blood flow and metabolic rates in rat brain. Thus FDG and DG appear to behave similarly as competitive substrates with glucose for membrane transport sites and hexokinase.

Because DG-6-PO_4 and FDG-6-PO_4 are not substrates for further metabolism through glycolysis, glycogen formation or the pentose shunt, they accumulate in tissue. The rate of accumulation or the net accumulation over a given period of time is proportional to the phosphorylation rate of exogenous glucose. This allows the isolation of the membrane transport and phosphorylation steps and their mathematical description using the principles of competitive enzyme reactions and tracer kinetics (3,9,10). Studies in dogs, monkeys and humans by Phelps et al (12,13) and in rats and dogs by Gallagher et al

(6,14) have shown that FDG is extracted and converted to FDG-6-PO_4 in the myocardium and suggest that FDG could be used to measure the rate of exogenous glucose utilization in the heart.

In the present study, we have investigated the use of FDG, the tracer kinetic model developed in our laboratory (9,10) as an extension of the Sokoloff model (3) and PCT for the determination of the local myocardial rate of glucose metabolism in vivo. These studies in dogs were performed to determine 1) the kinetic constants for transport and phosphorylation of FDG and dephosphorylation of FDG-6-PO_4; 2) the lumped constant; and 3) to examine the stability of the model over a wide range of glucose metabolic rates and in states of severe mismatches in myocardial blood flow and glucose metabolism.

MATERIALS AND METHODS

Preparation of FDG:

FDG with a specific activity of 10-20 mCi per mg was synthesized by the method developed by Ido et al (4) and modified by Barrio et al (15). The radiochemical purity, as assayed by thin layer liquid chromatography, was greater than 95%.

Animal preparation:

Ten mongrel dogs weighing 20 to 30 kg were anesthetized with sodium pentobarbital (25mg/kg, iv), and small supplemental doses were administered as required. The animals were intubated and ventilated with room air using a Harvard respirator. Catheters were advanced through both femoral arteries into the aorta for monitoring systemic blood pressure and withdrawal of arterial blood for measurements of blood flow with radioactive microspheres. A thoracotomy was performed in the fifth left intercostal space, the pericardium incised widely and sutured to the chest wall to form a cradle in which

the heart was suspended. Two polyethylene cannulae were inserted through a puncture wound into the left atrium and used for injection of radiolabeled microspheres and arterial blood sampling. A third catheter was inserted in the coronary sinus for venous blood sampling. ECG and systemic blood pressure, measured through the aortic catheter with a Statham P23 Db pressure transducer, were recorded continuously on a strip chart recorder.

Two dogs were prepared as described above but in addition a mechanical occluder was placed on the left circumflex artery (LCX). Blood flow through the LCX was continuously monitored with an electromagnetic flow probe (Series 500, Biotronix) placed proximal to the constrictor. A 30 gauge needle connected to fine plastic tubing (Lymphangiography Set No. 6677, Becton-Dickinson) was inserted into the LCX in order to induce coronary hyperemia by a bolus injection of the vasodilator papavarine (1 mg).

Blood samples:

10 mCi of FDG was injected intravenously over a 30 second interval and arterial and venous blood samples obtained; starting at time zero, samples were withdrawn every 15 seconds for 3 minutes and every minute for the next 12 minutes. The sampling interval was then progressively lengthened over the next 3 hours. Every sample was divided into two aliquots, one for measurement of FDG activity in whole blood, while the other one was immediately placed into an ice bath for measurement of FDG plasma activity and plasma glucose concentrations. FDG activity was measured in a well counter and corrected for radioactive decay. Plasma glucose levels were measured by standard enzymatic techniques. Additional arterial and venous samples were taken at the beginning, middle and end of each experiment for the measurement of free fatty acid and lactic acid concentrations, hematocrit and blood gases.

Arterial and coronary sinus venous plasma activity were used to calculate the myocardial tissue activity curve by the Fick method. This was

accomplished by integration of the A-V difference multiplied by the plasma flow (plasma flow = whole blood flow x (1-hematocrit)) over time. This measurement of the myocardial time activity curve was then compared to the tissue curve obtained from the myocardial activity measured by PCT.

Measurement of myocardial blood flow:

Regional myocardial blood flow was determined with radioactive carbonized polystyrene microspheres (15 ± 3 u) using the arterial reference sample technique (16) at the beginning (Co-57) and at the end (Sn-113) of each experiment. The details of this approach are presented elsewhere (17).

Tomographic imaging:

After instrumentation, each dog was carefully positioned in the UCLA positron computed tomograph, ECAT (18, Ortec, Inc., Oak Ridge, Tennessee). A low power neon laser was used in order to identify an optimal cross-section through the left ventricle. After recording a transmission scan for subsequent correction of photon attenuation, a blood pool image was acquired for two minutes after in vivo labeling of red blood cells by inhalation of O-15 carbon monoxide. The blood pool image was used to correct the myocardial F-18 tissue activity for cross contamination from FDG activity in the blood pools and the blood activity in myocardial tissue. To allow for sufficient decay of O-15 (halftime 2.04 minutes), FDG was injected 15 minutes later. Starting at the time of injection, serial images were recorded at the same level across the heart: an initial set of ten 2-min images was followed by ten 5-min images and by ten 10-min images, resulting in a total scanning time of 3 hours. All image data were collected in the medium resolution mode with an image resolution of 1.6 cm full width half maximum. Also, in order to reduce the blurring effect of cardiac motion, the images were acquired in a gated mode of the diastolic phase of the cardiac cycle. All images were decay corrected and normalized to the same acquisition time.

The tomograph was calibrated following each experiment with a 20 cm diameter cylindrical phantom containing a known amount of positron activity. A known volume (measured with calibrated pipets) of activity from the calibration phantom was counted in a well counter along with the blood samples. The ratio of the counts/time/volume in the well counter to the counts/time/volume of the cylinder in the tomograph provides a calibration factor that relates the tomographic measurement of the myocardial activity to the activity of the blood samples measured in the well counter (9).

After reconstruction of the cross-sectional images, regional myocardial F-18 concentrations were measured as follows: Six regions of interest, usually 0.428 cm^2 large (37 pixels), were assigned to each of the 30 images of the myocardium of each experiment. A seventh region of interest was placed in the center of the ventricular cavity in each image in order to measure the blood pool activity. Within the regions of interest, the mean counts/pixel were determined. The same regions of interest were also assigned to the O-15 CO blood pool image in order to evaluate the amount of contamination from blood activity in each of the myocardial tissue regions. The F-18 tissue data were then corrected for a spillover from blood activity using:

$$^{18}F(t)_i = \frac{(C^{15}O)_i}{(C^{15}O)_c} \quad \frac{(C^{15}O)_{bl}}{^{18}F(t)_{bl}} \quad ^{18}F(t)_c \qquad (1)$$

Where $(C^{15}O)_i$ is the O-15 activity concentration in the myocardial region of interest measured with the PCT. The terms $(C^{15}O)_c$ and $^{18}F(t)_c$ are the O-15 and F-18 activity concentration in a region of interest located in the center of the left ventricular chamber of the PCT images. The terms $(C^{15}O)_{be}$ and $^{18}F(t)_{bl}$ are the activity concentrations in the blood samples as measured in a

well counter for a known volume of blood. The terms involving F-18 are determined as a function of time t because the activity concentrations of F-18 in tissue and blood are changing with time. Equation 1 allows the calculation of the local F-18 activity in the image ($^{18}F(t)_i$) of the myocardium due to spillover of activity from blood chambers and that due to activity in the vascular space of the myocardium itself. These values are calculated for each region of interest and are subtracted from the corresponding tissue F-18 concentration to allow the determination of the interstitial FDG plus FDG-6-PO_4 concentrations.

A second correction was needed because of the object size related partial volume effect (19) which causes an underestimation of the isotope concentrations on the PCT images if the size of the object is close to or smaller than the resolution of the tomograph. The recovery coefficients (RC) used to correct for this partial volume effect have been established initially in phantom studies by Hoffman et al (19) and their use for in vivo measurements was subsequently confirmed by Wisenberg et al (20). The RC is the apparent isotope concentration in the image divided by the true isotope concentration; its value is 1 for large objects in which image concentration is equal to the true object concentration. These corrections require knowledge of the myocardial wall thickness which was determined in vivo by echocardiography and post mortem as follows. At the end of each experiment, the plane of the cross-sectional image was identified on the heart with the aid of the low power neon laser and was carefully marked on the surface of the left ventricle. The dogs were then sacrificed with a high concentrated KCl, the heart was removed and a 1.6 cm thick slice taken at the level of the PCT image. The shape of this slice was then drawn at a 1 to 1 scale. The wall thickness was measured at the level of each region of interest on the images, and the data divided by the corresponding recovery coefficient.

Calculation of the rate constants, lumped constant and glucose metabolic rate

As demonstrated previously for the brain (7,9,10), the myocardial metabolic rate of glucose (MMRGlc) from exogenous sources can be derived from the kinetics of FDG using an extension of the Sokoloff model (3) by Phelps and Huang (9,10). This model assumes three compartments, viz, a plasma compartment, a compartment for glucose and FDG in tissue, and a compartment for phosphorylation of glucose and FDG to glucose-6-PO_4 and FDG-6-PO_4 in tissue (Figure 1). These three compartments are referred to as compartments 1, 2, and 3, respectively. The boundary between compartments 1 and 2 consists of the capillary and cell membranes. Compartments 2 and 3 are not separated by a physical barrier but by the phosphorylation ratio catalyzed by hexokinase and dephosphorylation by phosphatase. Thus, the capillary and cell membranes are lumped together in the form of the operational model equation of Sokoloff et al (3) and Phelps and Huang et al (9,10).

In this model, if FDG-6-PO_4 is trapped in compartment 3 and its concentration is directly related to MMRGlc. The terms k_1^* to k_4^* (Figure 1) are first order rate constants which can be determined using the operational equation of the model (9,10) if the rate of change of total tissue F-18, plasma FDG and plasma glucose concentration are known as a function of time. The time dependent F-18 tissue concentration curves were obtained by two methods: By PCT imaging and blood sampling to determine the arterial-venous FDG difference across the heart as a function of time (i.e. see Figure 9). Determination of the plasma glucose concentrations from the arterial blood samples. These values are then used to calculate the values of the k^*s by a least-squares estimation routine. The operational equations of the model and description of the analysis are given elsewhere (9,10).

Assuming k_4^* small (i.e low enzyme activity of phosphatase which hydrolyzes FDG-6-PO_4, (20)) and knowledge of the specific rate constants of the model, the metabolic rate of glucose can be calculated according to the formula (9,10).

$$MMRGlc = \frac{[Glc]}{LC} \quad k_3^* k_1^*/(k_1^*/(k_2^* + k_3^*) \qquad (2)$$

where [Glc] is the capillary plasma glucose concentration and LC is the lumped constant which accounts for difference in transport and phosphorylation between FDG and glucose. The term $k_3^* \times k_1^*/(k_2^* + k_3^*)$, which describes the combination of transport and phosphorylation of FDG will be referred to as a single term K. The value of LC has been shown to be equal to (9,10).

$$LC = \frac{[Glc]\ k_3^*\ k_1^*/(k_2^* + k_3^*)}{MR_f} \qquad (3)$$

where MR_f is the metabolic rate of exogenous glucose measured according to the Fick principle

$$MR_f = MBF\ (A-V) \qquad (4)$$

where MBF is the myocardial blood flow and A and V are arterial and venous plasma concentrations of glucose.

Uncoupling of flow and metabolism

The independence of the FDG model from myocardial blood flow (MBF) was examined in the following manner. Local MBF was increased by intracoronary administration of papaverine (1 mg) into the LCX without producing a signifi-

cant change in metabolism (22). This produced a condition of high local MBF and normal local metabolism in the distribution of the LCX. During this state $^{13}NH_3$ and labeled microspheres (I-125) were injected into the left atrium, 5 min allowed for equilibration of $^{13}NH_3$, and a PCT image of the myocardium recorded. After 70 min, the papaverine administration was repeated, FDG (5 mCi) was injected intravenously and microspheres (Cs-141) were injected into the left atrium. PCT and blood sampling were performed to estimate the rate constants and MMRGlc as described above.

This same sequence was repeated except that hyperemia was induced by occluding the LCX for 30 min and then releasing the occluder to produce reactive hyperemia. At the peak of the hyperemic MBF response (determined with the electromagnetic flow probe), FDG and labeled microspheres were injected intravenously into the left atrium, respectively. The reactive hyperemia after a 30 min total occlusion produces a state of high MBF and low glucose metabolism (about 30 to 50% of control values for 10 to 20 min) due to residual tissue acidosis (23). The MMRGlc was calculated using the directly measured rate constants and equation 2.

RESULTS

A typical example of a kinetic study is shown in Figure 2. Sixteen out of thirty serial images obtained at the same cross sectional level over a 200 min period after injection are shown on the left of Figure 2. The kinetic tissue data on the right of Figure 2 were obtained from 6 regions of interest in the left ventricle. The counts in these 6 regions were also averaged and the best fit of least squares analysis was plotted. The initial part of the curve, corresponding to the early images where blood activity is high and myocardial activity low, is contaminated by blood pool activity. Correction for this contamination was performed in all experiments using the spillover

fraction, obtained from the O-15 CO blood pool image for each region of interest, and the blood F-18 activity at the time of each scan. Blood activity could not be measured directly from the images because of a reverse contamination from myocardial activity into the blood activity in the cardiac chambers. The activity measured in the center of the ventricular cavity agreed with the value obtained from arterial blood samples only at the very early time when there was a high ratio of blood to myocardial activity (Figure 3).

The spillover fraction measured on the blood pool image by taking the ratio of activity in each region of interest to activity in the center of the ventricle, averaged 0.36 ± 0.12 SD and ranged from 0.19 to 0.56 for values throughout the myocardial sections and for all dog experiments.

The data of each region of interest were further corrected for a partial volume using the recovery coefficient predetermined in phantom studies (19) and corresponding to the thickness of the myocardium. The effect of both corrections are shown in Figure 4. The correction for blood pool spillover shown in Panel B resulted in a more realistic curve of early myocardial tissue uptake of FDG. Panel C shows the same data after correction for the partial volume effect. This latter correction significantly reduced the scatter in the values from different regions of interest. The mean curve shows a higher total tissue uptake than in Panel A, indicating that without the partial volume correction, the uptake rate and total tissue radioactivity concentration were underestimated. This of course results in an underestimation of the MMRGlc (i.e. only the metabolic rate obtained from the corrected curve was in agreement with the metabolic rate obtained by the Fick method).

The effect of the spillover of activity from the chamber to the myocardium was also greatest when the MMRGlc was low. This is illustrated by the studies

in Figure 5 and 6 where the values of the MMRGlc were 5.08 and 19.9 mg/min/100 gms, respectively. This results from the fact that as higher MMRGlc increases, the rate of formation and total amount of the FDG-6-PO_4 also increases compared to the surrounding activity as is apparent in the images and numerically in the curves of Figures 5 and 6.

Blood activity of FDG:

FDG clears rapidly from the arterial and venous blood, as shown in Figure 7. The expanded time scale of the early portion of the curve shows the delay between the arterial and the venous peak of activity. This delay averaged 0.24 ± 0.04 mins and represents the combination of blood transit time across the heart and the rapid forward and reverse exchange between blood and interstitial space due to the changes in the blood to tissue concentration gradient as a function of time after injection.

Metabolic rate and lumped constant (LC)

The tissue curves obtained from the images were used to estimate k_1^* to k_4^* of our compartmental model (9,10). Due to the proportionally high values of the corrections applied to the data and the propagation of errors through these corrections (i.e. limitations imposed by the present PCT resolution) the true value of individual k's could not be satisfactorily estimated. However, the estimate of the combined rate constant K^*, which is the product of the rate constants of phosphorylation k_3^* times the distribution volume of FDG $[k_1^*/(k_2^*+k_3^*)]$, was found to be reliable and had minimum variability introduced by errors generated by the corrections. The term K^* is the fractional utilization constant (i.e. rate constant describing the fractional rate at which plasma FDG is transported across the capillary and cell membranes and phosphorylated). This constant was then used to calculate the lumped constant, LC, in each experiment according to equation 3. The results

obtained are listed in Table 1 . The same calculation was applied to the tissue curves obtained from arterial-venous (A-V) FDG plasma activity. An example of the comparison of the kinetic curves obtained from the same animal by PCT and A-V sampling is shown in Figure 8.

The mean value of 0.68 ± 0.1 for LC was used to recalculate the exogenous metabolic rate using equation 2 for each individual experiment. The metabolic rate calculated in this manner was compared with the metabolic rate of glucose determined by the Fick method. The excellent agreement between both measurements is shown in Figure 9A. Because the dietary state of the dogs was not controlled, a wide range of myocardial glucose metabolic rates was observed. The values ranged from 1.7 to 21.1 mg of glucose/min/100gm of tissue and reflects the capability of the myocardium to utilize alternate substrates such as free fatty acids and lactic acid to meet its energy requirements.

The MMRGlc was also calculated from both the PCT and A-V kinetic FDG data using eqation 2. These values were correlated with the estimates from the Fick method individually (9A,B) and in a combination (9C). Although each of these correlations have somewhat different slopes and intercepts, there was no statistically significant difference. Thus, the PCT estimates agreed very well with the measurements by the direct A-V sampling approach for FDG and by the Fick method.

Metabolism-Blood Flow Uncoupling

An example of the measurement of MMRGlc when glucose metabolism and MBF are uncoupled is shown in Figure 10. The $^{13}NH_3$ image shows the papaverine induced hyperemia (MBF = 490 ml/min/100gm as measured with microspheres) in the LCX distribution (arrow) as compared to the normal MBF (86 ml/min/100 gms) in the remainder of the cross section. The MMRGlc image with FDG under the same papaverine induced hyperemia shows the uniform and correct distribution

of glucose metabolism throughout the left ventricle even though the MBF in LCX distribution is about 5 times higher than the rest of the myocardium. Although papaverine has a positive inotropic effect and, hence, can alter myocardial metabolism, this effect would appear to be small in relation to the tremendous hyperemic response produced by the action of the smooth muscle relaxant papaverine. Further, as indicated by studies in isolated dog heart myocardium, a bolus administration of only 3 umoles would have only a minimal effect on myocardial metabolism (22).

The far right hand image shows the reduced glucose metabolism in the LCX segment resulting from occluding the LCX for 30 min and then releasing the occluder to produce reactive hyperemia. The prolonged coronary occlusion produces severe ischemia. At the time of reperfusion, reactive hyperemia in the tissue supplied by the LCX occurs while return of glycolysis to control levels is delayed because of the residual tissue acidosis (23). The calculated MMRGlc in LCX distribution was about 19% of the value in the remainder of the normal tissue. Mochizuki and Neely (23) found that 30 minutes of myocardial ischemia in the rat reduced exogenous glucose utilization to 30% of control with a very slow recovery over the 30 minutes of reperfusion. Thus, in this latter case, the FDG method estimates the reduced MMRGlc even though there is a large MBF-MMRGlc mismatch (i.e. MBF is increased 5.6 times and glucose metabolism is reduced by about a factor of 5 compared to control values. The serial PCT images showed a high FDG activity in the LCX segment initially, reflecting the high MBF and transport into tissue. However, the tissue activity rapidly decreased as the high MBF removed FDG from the tissue and only small amounts of FDG were phosphorylated because of the low glucose metabolic rate in the LCX distribution.

DISCUSSION

As shown in Table I, the LC estimated in each experiment did not vary significantly over a wide range of metabolic rates. Thus, the evaluation of local myocardial MMRGlc is feasible using a mean value of LC in the model. The calculated MMRGlc from the FDG model showed a good correlation with the value obtained by the Fick method (Figure 9). These findings indicate the reliability of the model in the evaluation of MMRGlc over a wide range of metabolic states.

The value of LC found in this work (0.67 ± 0.10) is higher than the values reported for the brain with DG in the rat of 0.483 (3) and monkey of 0.344 (11) or FDG in man of 0.420 (9,10). However, studies also performed in our laboratory (23) using the isolated perfused rabbit myocardium have yielded a value of 0.60 ± 0.10 (S.D.) for FDG which is in good agreement with the value reported here.

Estimation of the plasma input function by in vivo measurements of blood activity in the cardiac chambers with PCT requires good tomographic resolution and cardiac gating. At late times after injection of FDG, the spillover from activity in the myocardium produces a significant overestimation of the blood activity concentration.

The studies in which MBF and metabolism were uncoupled by large local increases in MBF with normal or severely reduced MMRGlc (Figure 10) illustrate the viability of the model under these demanding conditions. These results provide experimental confirmation of the postulated low sensitivity of the model to changes in blood flow (3,9,10).

In this work, the values for the transport, phosphorylation and dephosphorylation rate constants were estimated from the time course of the plasma FDG concentration and the myocardial F-18 tissue activity concentration with

PCT or with A-V sampling technique for measuring the temporal sequence of FDG tissue uptake. The values of the rate constants (i.e. k_1^*, k_2^*, k_3^* and k_4^*) estimated from both sets of data using least squares curve fitting to our model produced comparable results. Reasonable convergence was usually achieved within 20 iterations. In some studies we experienced a slower convergence and greater difficulty in obtaining reasonable values for the individual rate constants. However, the value of the factor $k_1^* k_3^*/(k_2^* + k_3^*)$ was found to be very insensitive to the exact fitting results. In other words, the value of the factor $k_1^* k_3^*/(k_2^* + k_3^*)$ converges rapidly and is quite insensitive to the initial values chosen for the curve fitting. This allowed accurate estimates of local MMRGlc to be determined even though unsatisfactory estimates of the individual constants was found.

The large variation in the values of the individual rate constants is to be expected in this study with such large variations in MMRGlc (i.e., 1.7 to 21.1 mg/min/100gms) but the numerous correction factors employed produced uncertainties in the data that added inaccuracies to the estimates of the individual constants. This was most apparent in fitting the early part of the tissue curves (i.e., the first 25 min) when F-18 uptake in tissue increases most rapidly. Also, the early part of the tissue curve is most sensitive to errors in the corrections applied to the data for the contamination of the tissue data from blood pool activity. The correction for the underestimation of tissue activity due to a partial volume effect was performed by multiplying the data by recovery coefficients that ranged from 1.6 to 2.5. Thus, these corrections were of sufficient magnitude that inaccuracies in their values would produce significant errors.

The validity of these corrections however can be assessed in two ways: First, only the MMRGlc obtained from the corrected curves showed a good correlation with the MMRGlc obtained using the Fick method (Figure 9). Second, in

all our experiments the corrected tissue curve determined with PCT matched the tissue curve obtained by integrating the A-V difference of FDG in plasma as shown in a typical case in Figure 8. The uncorrected tissue curve systematically showed an underestimation of the total activity in tissue due to the partial volume effect and a slow rate of increase at the early times due to contamination from blood activity.

These corrections are directly related to the resolution of the tomograph, and an improvement of the resolution will significantly reduce their magnitude, and a more reliable evaluation of the individual rate constants can be expected.

REFERENCES

1. Phelps ME, Hoffman EJ, Mullani NA, et al: Application of annihilation coincidence detection to transaxial reconstruction tomography. J Nucl Med 16:210-223, 1975.

2. Phelps ME: Emission computed tomography. Sem Nucl Med 7:337-365, 1977.

3. Sokoloff, LM, Reivich C, Kennedy MH, Des Rosiers C, Patlak S, Pettigrew KD, Sakurada O and Shinohara M: The (C-14) deoxyglucose method for the measurement of local cerebral glucose utilization: theory. procedure, and normal values in the conscious and anesthetized albino rat. J Neurochem 28:897-916, 1977

4. Ido T, Wan WN, Casella V, et al: Labeled 2-deoxy-D-glucose analogs. ^{18}F-labeled 2-deoxy-2-fluoro-D-glucose, 2-deoxy-2-fluoro-D-mannose, and ^{14}C-2-deoxy-2-fluoro-D-glucose. J Label Compds Radiopharm 24:174-183, 1978.

5. Bessel EM, Foster AB, Westwood JH: The use of deoxyfluoro-D-glucopyranoses and related compounds in a study of yeast hexokinase specificity. Biochem J 128:199-204, 1972.

6. Gallagher BM, Ansari A, Atkins H, et al: Radiopharmaceuticals XXVII. ^{18}F-labeled 2-deoxy-2-fluoro-D-glucose as a radiopharmaceutical for measuring regional myocardial glucose metabolism in vivo: Tissue distribution and imaging studies in animals. J Nucl Med 18:990-996, 1977.

7. Reivich M, Kuhl D, Wolf A, et al: The (^{18}F) fluorodeoxyglucose method for the measurement of local cerebral glucose utilization in man. Circ Res 44:127-137, 1979.

8. Machado DeDomenech EE, Sols A: Specificity of hexokinases towards some uncommon substrates and inhibitors. FEBS letters 119:174-176, 1980.

9. Phelps ME, Huang SC, Hoffman EJ, et al: Tomographic measurement of local cerebral glucose metabolic rate in man with 2-(^{18}F) fluoro-2-deoxy-D-glucose. Validation of method. Ann Neurol 6:371-388, 1979

10. Huang SC, Phelps ME, Hoffman EJ, et al: Noninvasive determination of local cerebral metabolic rate of glucose in man. Am J Physiol 238:E69-E82, 1980

11. Kennedy, C, Sakurada O, Shinohara M, et al: Local cerebral glucose utilization in the normal conscious macaque monkey. Ann Neurol 4:293-301, 1978

12. Phelps ME, Hoffman EJ, Selin C, et al: Investigation of ^{18}F-2-deoxyglucose for the measurement of myocardial glucose metabolism. J Nucl Med 19:1311-1319, 1978.

13. Phelps ME, Schelbert HR, Hoffman EJ, et al: Physiologic tomography studies of myocardial glucose metabolism, perfusion and blood pools with multiple gated acquisition. Advances in Clin Card Vol 1:373-393, 1980.

14. Gallagher BM, Fowler JS, Gutterson NI, et al: Metabolic trapping as a principle of radiopharmaceutical design: Some factors responsible for the biodistribution of (F-18)-2-deoxy-2-fluoro-D-glucose. J Nucl Med 19:1154-1161, 1978.

15. Barrio JR, MacDonald NS, Robinson GD Jr, et al: Remote, semiautomated production of F-18 labeled 2-deoxy-2-fluoro-D-glucose. J Nucl Med 22:372-375, 1981.

16. Heymann MA, Payne BD, Hoffman JIE, et al: Blood flow measurements with radionuclide-labeled particles. Prog Cardiovasc Dis 20:55, 1977

17. Schelbert HR, Phelps ME, Hoffman EJ, et al: Regional myocardial perfusion assessed by N-13 labeled ammonia and positron emission computerized axial tomography. Am J Cardiol 43:208-218, 1979

18. Phelps ME, Hoffman EJ, Huang SC, et al: ECAT: A new emission computerized tomographic imaging system for positron emitters in radiopharmaceuticals. J Nucl Med 19: 635-647, 1978.

19. Hoffman EJ, Huang SC, Phelps ME: Quantification in positron emission computed tomography. I. Effect of object size. J Comput Assist Tomogr 3:299-308, 1979.

20. Wisenberg G, Schelbert HR, Hoffman EJ, et al: In vivo quantitation of regional myocardial blood flow by positron-emission computed tomography. Circ 63:1248-1258, 1981.

21. Anchors JM, Haggerty DF and Karnovsky ML: Cerebral glucose-6-phosphatase and the movement of 2-deoxy-D-glucose across cell membranes. J Biol Chem 252:7035-7041, 1977

22. Endoh M and Homma M: Effects of papaverine and its interaction with isoprenaline and carbachol on the contractile force and cyclic nucelotide levels of the canine ventricular myocardium. Naunyn-Schmiedeberg's Arch Pharmacol 299:241-248, 1979

23. Mochizuki S, Neely JR: Energy metabolism during reperfusion following ischemia. J Physiol 76:805-812, 1980.

24. Krivokapich J, Huang SC, Phelps ME, et al: Measurement of rabbit myocardial metabolic rate of glucose in vitro using ^{18}F-2-fluoro-2-deoxy-D-glucose. *Am J Physiol (Submitted).*

LEGENDS

Figure 1: Schematic illustration of the compartmental tracer kinetic model for FDG. The terms C_p^*, C_E^* and C_M^* are the concentrations of FDG in plasma and tissue and FDG-6-PO_4 in tissue, respectively. The k^*'s are the rate constants for forward and reverse membrane transport (endothelium and cell), hexokinase mediated phosphorylation and phosphatase mediated dephosphorylation, respectively.

Figure 2: Left: Example of a series of tomographic images as a function of time for a single cross section through the heart after the intravenous injection of FDG. Examples are shown for 16 of the time intervals out of a total of 30. Right: Numerical data from this kinetic study showing the individual kinetic curves for 6 different regions (points) and also the mean value of the regions of interest (solid lines).

Figure 3: Example of the FDG blood curves comparing samples counted externally and measured in vivo with PCT.

Figure 4: Example of tissue kinetic curves showing the effect of correcting for blood pool spillover of activity into the myocardium and the partial volume effect. The points are individual regions of interest and the solid line is the mean value for the multiple regions of interest. Note that the correction for spillover has the most dramatic effect at the early portions of the tissue uptake curve. The partial volume correction elevates the entire curve and also has the most dramatic effect on the calculated metabolic rate (MR).

Figure 5: Left: selected tomographic images taken as a function of time after the intravenous injection of FDG in an animal with a low glucose metabolic rate. Note that the myocardium is not well delineated away from

surrounding activity and that in the blood pool of the cardiac chambers until about 30 min (compare to Figure 6). Right: Kinetic data from this study showing the impact of the spillover and partial volume correction when the glucose metabolic rate is low. Numbers at the bottom of the figure are the times of the scans in minutes. The two dimensional image at the bottom of the figure illustrates the transmission images (0 is anterior - posterior and 60° oblique views) used for setup of the dog for the PCT study.

Figure 6: Left: Tomographic images as a function of time after the intravenous injection of FDG when the glucose metabolic rate is high. Note rapid delineation of the myocardium away from the surrounding and blood pool activity due to the rapid sequestering of FDG-6-PO_4 in the myocardium. Times of the scans are shown at the bottom of the images. The 10 scans shown have been selected from a total of 40 images taken over a time period of 3 hours. Right: Kinetic data showing the impact of the blood pool spillover and partial volume correction when the metabolic rate is high. Note that the spillover correction at the early portions of the curve have less of an impact when the metabolic rate is high (compare to Figure 5).

Figure 7: Example of the arterial and venous (i.e. superior venacava) time activity curves across the heart after an I.V. injection of FDG. Note that FDG is rapidly cleared from the plasma. The arterial and venous curves to the left illustrate the time displacement and difference in magnitude due to transit across the heart and the forward and reverse diffusion of FDG from plasma and tissue and also the extraction of FDG which is subsequently phosphorylated and remains in the heart. Clearance curve at the right is for arterial plasma.

Figure 8: Example showing the comparison of the myocardial tissue uptake curves generated from the integral values of the arterial-venous FDG

difference across the heart (see method section) and recorded in vivo with PCT. FDG was injected intravenously.

Figure 9: A: Plot showing the correlation of the calculated glucose metabolic rate from the Fick method to that from the FDG model and rate constants generated from the tissue uptake curve using arterial-venous sampling of FDG. B: Same as A except the rate constants and the calculated glucose metabolic rate with FDG was determined with PCT. C: The combined data of Figures A and B. There was no statistically significant difference between the fits in A, B and C indicating the good correlation between the in vivo PCT estimates of the metabolic rate versus the direct sampling techniques employing the arterial-venous FDG sampling and the Fick method.

Figure 10: Study illustrating the flow independence of the FDG method. At left are the transmission scans showing the anatomical distribution in the cross section of the thorax (open area at the top of the images is due to the open-chest preparation). Numbers in the lower right-hand corner of the images are the flows in ml/min/100gm in the region of the myocardium supplied by the left circumflex artery as determined by the microsphere technique. The flow in the remainder of the left ventricle ranged from 85 to 90 ml/min/100 gm in each experiment. Anterior is at the left of the image and the left side of the cross section is at the bottom of the image.

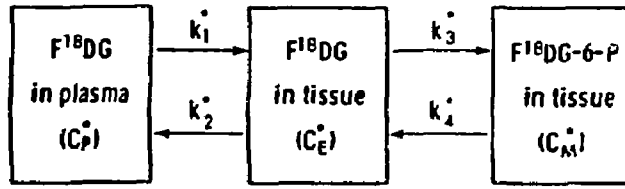

DIAGRAM OF THE THREE COMPARTMENTS IN FDG MODEL

Figure 1

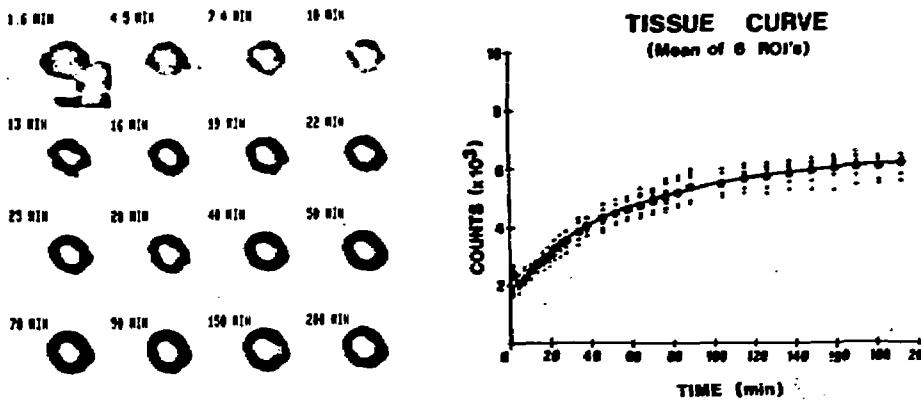

Figure 2

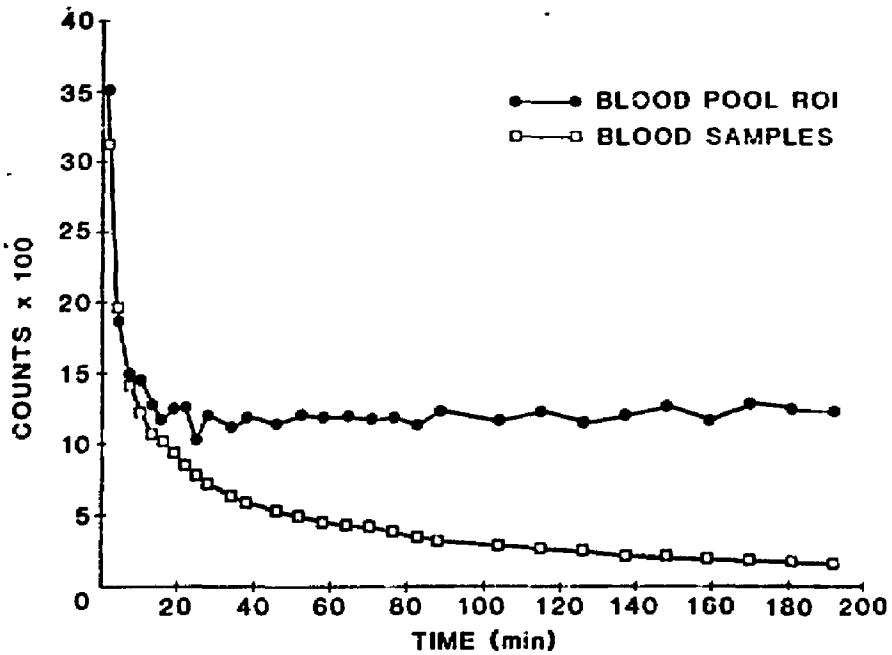

Figure 3

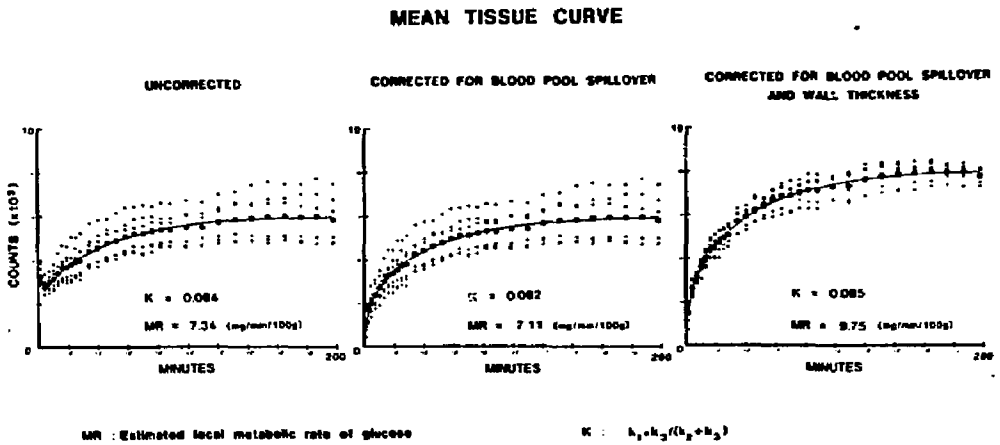

Figure 4

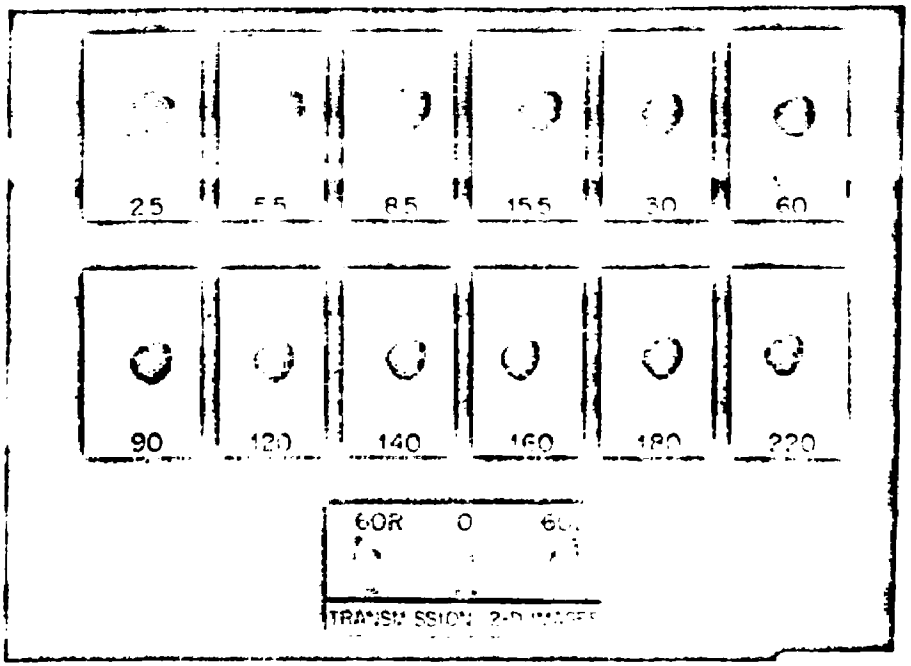

Figure 5A

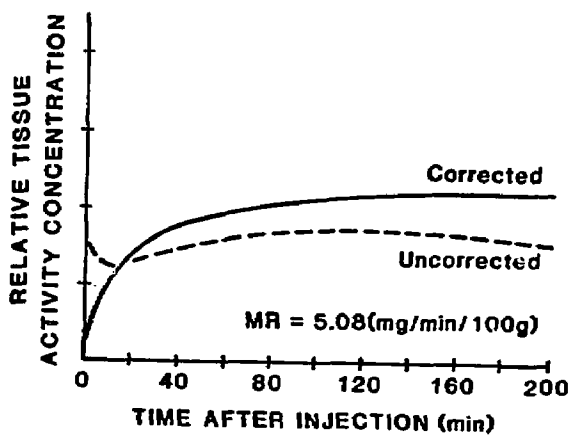

Figure 5B

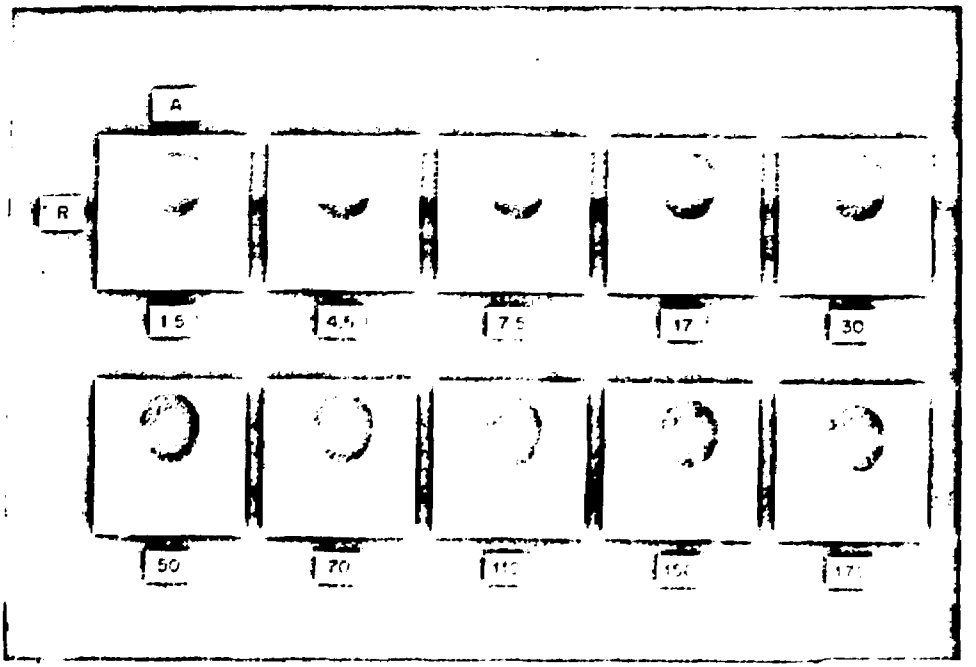

Figure 6A

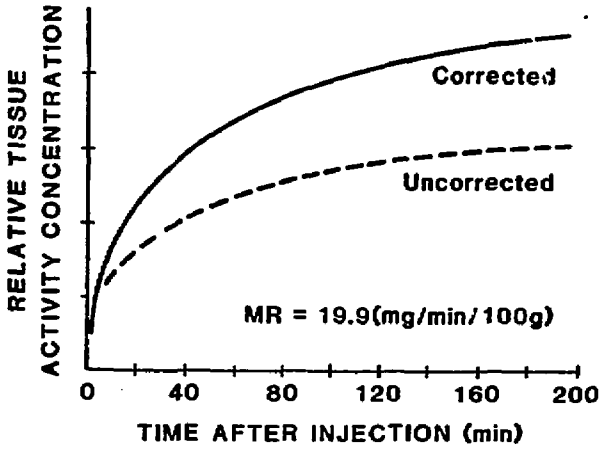

Figure 6B

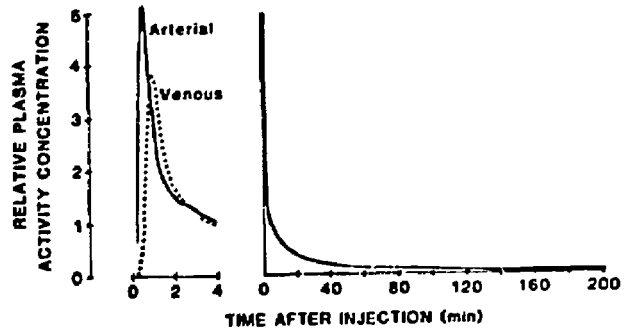

Figure 7

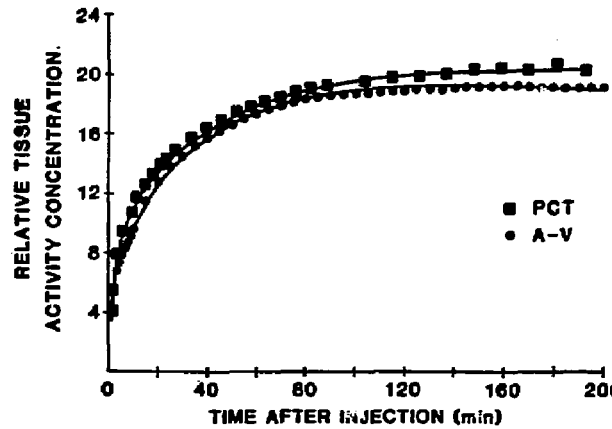

Figure 8

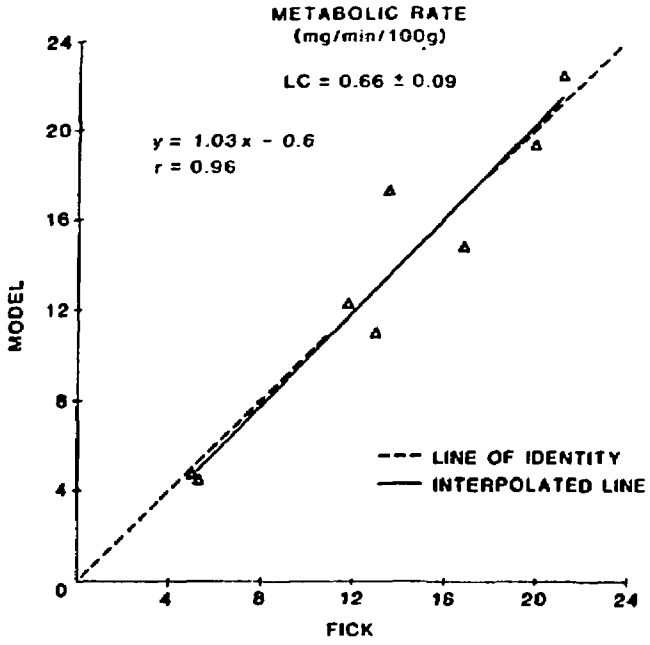

Figure 9A

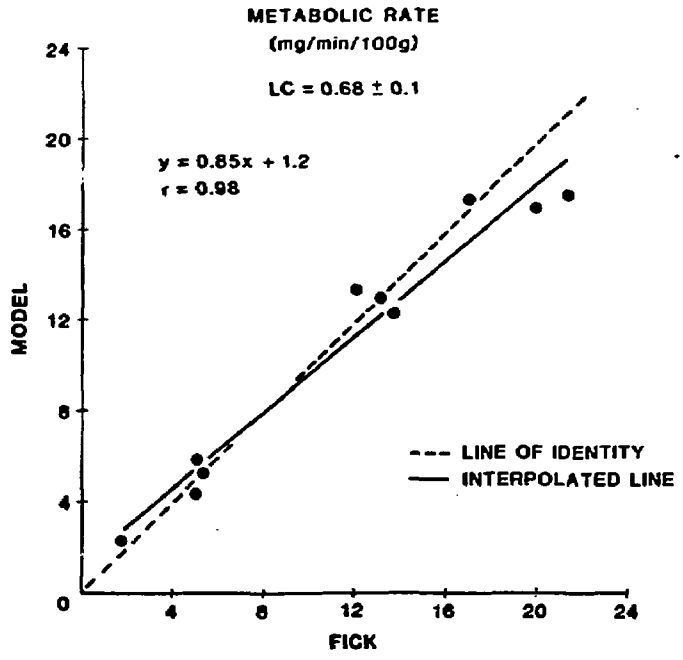

Figure 9B

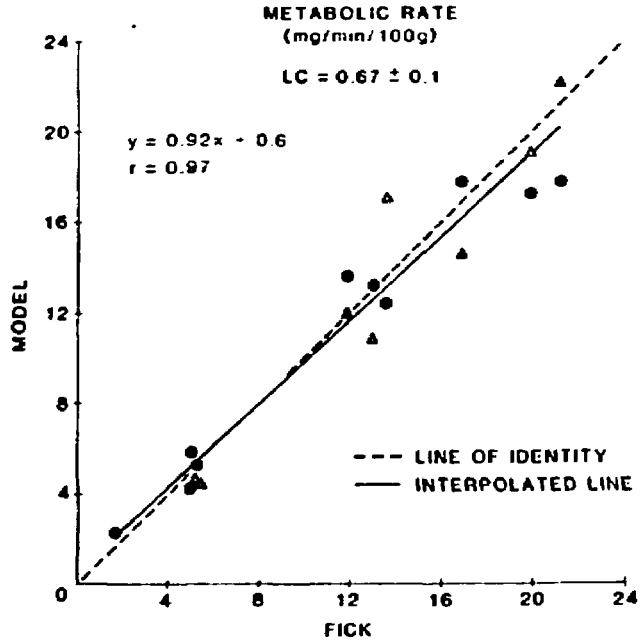
METABOLIC RATE
(mg/min/100g)
LC = 0.67 ± 0.1
y = 0.92x - 0.6
r = 0.97
MODEL
FICK
0
4
8
12
16
20
24
LINE OF IDENTITY
INTERPOLATED LINE

Figure 9C

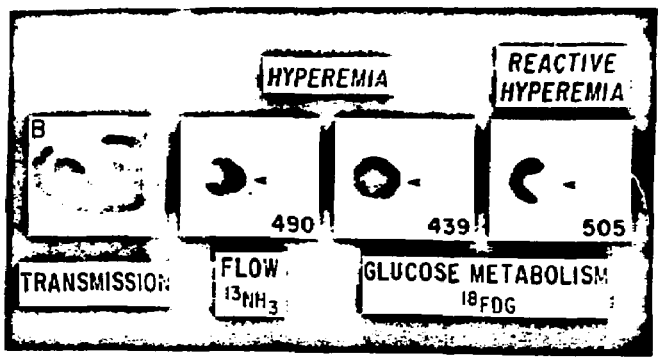
HYPEREMIA
REACTIVE HYPEREMIA
B
490
439
505
TRANSMISSION
FLOW
$^{13}NH_3$
GLUCOSE METABOLISM
^{18}FDG